Theory of laser-induced ultrafast magneto-optic spin flip and transfer in charged two-magnetic-center molecular ions: Role of bridging atoms

Chun Li, Wei Jin, Hongping Xiang, Georgios Lefkidis, and Wolfgang Hübner

Phys. Rev. B **84**, 054415 — Published 5 August 2011

DOI: 10.1103/PhysRevB.84.054415

Theory of laser-induced ultrafast magneto-optic spin flip and transfer in charged two-magnetic-center molecular ions: role of bridging atoms

Chun Li*
School of Mechanics, Civil Engineering and Architecture, Northwestern Polytechnical University, Xi'an 710072, China

Wei Jin, Hongping Xiang, Georgios Lefkidis, and Wolfgang Hübner
Department of Physics and Research Center OPTIMAS, University of Kaiserslautern, PO Box 3049, 67653 Kaiserslautern, Germany

(Dated: June 1, 2011)

Laser-induced ultrafast spin manipulations in positively charged two-magnetic-center molecular ions with a small number of bridging atoms are investigated to explore the role of bridging atoms in the spin switching process and spin transferability between the magnetic centers via the Λ process. Taking O and Mg as examples for bridging atoms, fully *ab initio* calculations demonstrate that spin flip can be readily achieved on subpicosecond time scales at both magnetic centers of the linear structures composed of two nonidentical magnetic atoms with a single bridging atom in between. Although these two nonmagnetic elements possess completely different chemical and electronic natures, both types of bridging atoms contribute to spin density redistribution at the magnetic atoms, especially for the low-lying triplet states that are suitable to act as initial and final states in the Λ-type process of spin flip or transfer. This also provides a rule-of-thumb that spins in the linear structures can be flipped more easily since symmetric structures exhibit weaker magnetocrystalline anisotropy. The spin transfer process achieved in the structure [Fe-O(Mg)-Co]$^+$ demonstrates that if both bridging atoms are involved to further lower the symmetry of the linear structures, spin transferability between the Fe and Co atoms can be improved.

PACS numbers: 75.78.Jp, 78.20.Ls, 78.67.-n

I. INTRODUCTION

With the development of femtosecond lasers, ultrafast magnetization dynamics has become one of the most important issues of modern magnetism to fit the technological demand on smaller sizes and shorter time scales in magnetic responses.[1,2] In this quest, the optical manipulation of the magnetization promises to become a real alternative to the magnetic field pulses. Since the ultrafast all-optical demagnetization in ferromagnetic materials was discovered,[3] various light-driven scenarios and mechanisms have been proposed.[4,5] Theoretical investigation showed that the femtosecond relaxation of the magneto-optical response results from exchange interaction and spin-orbit coupling (SOC).[6] Subsequent studies have demonstrated that subpicosecond spin dynamics in electronically correlated magnetic materials can be realized by exploiting the ultrafast electron-photon interaction.[7,8]

Small magnetic nanostructures and molecules are promising building blocks for quantum technologies, due to their reproducible nature and ability to self-assemble into complex structures.[9] These nanostructures are also good candidates for spin-flip and spin-transfer devices since they form natural narrow-band systems well suited for the symmetry selection of magnetic target states and provide great potential for coherent spin manipulation.[10] Especially multi-magnetic-center structures can be regarded as good prototypes for the future realization of logic functionality in nanoscale devices.[11]

The basic necessity for any logic functionality of these structures is the possibility to not only flip the spin locally but also transfer the spin from one center to another. Recent investigations have shown that ultrafast laser-induced spin flip or spin transfer can be achieved in one-, two-, and three-magnetic-center structures via the Λ process.[11–15] However, it was found that while spin flip is relatively easy, spin transfer is much harder to be achieved. That is, only a relatively small subset of the investigated molecules exhibited spin transfer while the majority did not. Therefore, a systematic first-principles quantum mechanical wave-function investigation of this question is a timely endeavor in research. In particular, there is no current knowledge of how the bridging of adjacent magnetic centers affects the spin transferability and the logic functional operability of multicenter magnetic molecules besides the tremendous need.

According to our theoretical work in recent years, in order to achieve ultrafast laser-induced spin manipulation through a Λ process, the separation, both spatial and energetic, between the involved magnetic centers has to be neither too small nor too large. Fig. 1 shows a sketch of the needed energy differences between initial and final states and between the initial state and the intermediate state in the Λ process. Firstly, the energy difference between initial and final states must differ by at least 1 cm^{-1}, otherwise the two states cannot be distinguished (e.g. in difference spectroscopy) and they will be thermally equally populated. But this difference should not become too large either, in order to avoid fast direct relaxation channels. At the same time, the energy difference between the ground states and the excited state must be larger than 0.5 eV, so that the optical transitions between the ground states and the excited state are sufficiently fast. On the other hand, if the energy difference between the ground and the target excited states is too large, the detuning to the adjacent excited states is small, and hence they will be substantially addressed by the same laser pulse as well, leading to undesired interference effects. From Fig. 1 we can see that the middle area is ideal for the Λ process. Following the aforementioned trail of thoughts, in order to improve the spin transferability, it is a good idea to separate the magnetic centers with a small number of bridging atoms (localization of the spin but delocalization of the charge). The nature of these bridging atoms will influence the overlap between the magnetic centers.

In this manuscript, ultrafast laser-induced spin flip and spin transfer in positively charged two-magnetic-center molecular ions with a small number of bridging atoms are systematically investigated using fully *ab initio* calculations. Firstly, the theoretical model of the Λ process and its detailed solution procedure are introduced in Section II. This approach is then applied to a family of structures to examine the role of bridging atoms in the spin flip/transfer processes. The obtained theoretical results show that the use of bridging atoms can enhance Λ processes (Section III).

II. THEORY AND TECHNICAL DETAILS

For the Λ-process scenarios leading to spin switching and transfer we use a real-space quantum chemistry approach, which, contrary to momentum-space methods, enables us to find localized d-states of the magnetic molecules. Moreover, correlations play a crucial role in our systems and real-space methods are more suitable to describe their complex electronic structure. Additionally, we wish not only to calculate the energy levels but also the wavefunctions and the elements of the optical transition matrix (electric-dipole elements) which are necessary for the time-propagation step.

In order to properly describe the laser-matter interaction, as demonstrated in previous works,[12,13,16] the Hamiltonian of the interacting system is solved in the following three steps: The first step is to solve the Hamiltonian of a magnetic

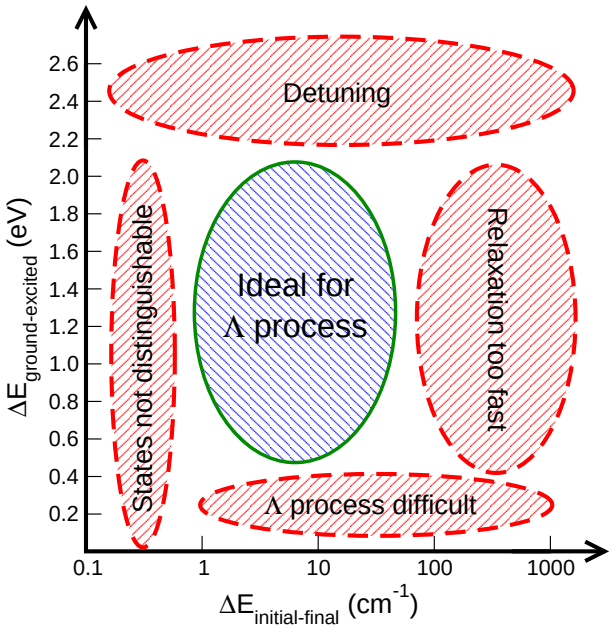

FIG. 1. (Color online) Sketch of the required energy differences between initial and final states (abscissa axis in logarithmic scale) and between the initial state and the intermediate excited state (ordinate axis) in the Λ process.

material without external field:

$$H^{(0)} = -\frac{1}{2}\sum_{i=1}^{N_{\rm el}}\nabla^2 - \sum_{i=1}^{N_{\rm el}}\sum_{a=1}^{N_{\rm at}}\frac{Z_a}{|\mathbf{R}_a-\mathbf{r}_i|} + \\ + \sum_{i=1}^{N_{\rm el}}\sum_{j=1}^{N_{\rm el}}\frac{1}{|\mathbf{r}_i-\mathbf{r}_j|} + \sum_{a=1}^{N_{\rm at}}\sum_{b=1}^{N_{\rm at}}\frac{Z_a Z_b}{|\mathbf{R}_a-\mathbf{R}_b|}, \tag{1}$$

where $N_{\rm el}$ and $N_{\rm at}$ are the number of electrons and atoms, $\mathbf{r}_i$ and $\mathbf{r}_j$ the position vectors of the electrons, $\mathbf{R}_a$ and $\mathbf{R}_b$ are the position vectors of the atoms, and Z_a and Z_b are the charges of the nuclei. In this step, the electronic correlation term (the third term on the right-hand side) is the most important one and should be carefully dealt with. One main aspect of our theory is the use of triplets in the Λ processes, because in this way we can separate spin and charge dynamics (triplets are built of at least two unpaired electrons, while for doublets one single electron can act as a common carrier for both charge and spin). Last but not least, spin redistribution requires less energy than charge redistribution, and triplets work better also for the reason that it is easier to find excited states for which the two transition-matrix elements (between the ground and excited states) are of similar magnitude.[17] In the calculations, the symmetry-adapted cluster configuration interaction (SAC-CI)[18] method implemented in GAUSSIAN 03 is adopted in this step to obtain accurate many-body wavefunctions, including electronic correlations at high level.[19]

The second step is a time-independent perturbative step, in which the SOC and the static external magnetic field $\mathbf{B}_{\rm stat}$ are switched on. The corresponding Hamiltonian is:

$$H^{(1)} = \sum_{i=1}^{N_{\rm el}}\frac{Z_a^{\rm eff}}{2c^2R_i^3}\mathbf{L}\cdot\mathbf{S} + \sum_{i=1}^{N_{\rm el}}\mu_L\mathbf{L}\cdot\mathbf{B}_{\rm stat} + \\ + \sum_{i=1}^{N_{\rm el}}\mu_S\mathbf{S}\cdot\mathbf{B}_{\rm stat}, \tag{2}$$

where relativistic effective nuclear charges $Z_a^{\rm eff}$ are used for the SOC. $\mathbf{L}$ and $\mathbf{S}$ are the orbital and spin momentum operators, respectively, μ_L and μ_S are their respective gyromagnetic ratios, and c is the speed of light. Note that all the terms in Eq. (1) and the first term in Eq. (2) are intrinsic properties of the material and do not depend on any experimental parameters.

The effect of the time-dependent laser pulse can be taken into account by means of a time-dependent vector potential $\mathbf{A}_{\rm laser}(t)$ (minimal coupling). The corresponding exact Hamiltonian can be written as:

$$H^{(2)}(t) = \mathbf{p}^{(1)}\cdot\mathbf{A}_{\rm laser}(t) + \mathbf{S}\cdot\mathbf{B}_{\rm laser}(t). \tag{3}$$

This is the third step, in which a suitably tailored laser field with a simple $sech^2$-shaped envelope is used, $\mathbf{p}^{(1)}$ is the electron momentum as obtained from the combination of the unperturbed Hamiltonian $H^{(0)}$ and the perturbation term $H^{(1)}$. $\mathbf{B}_{\rm laser}(t)$ is the time-dependent magnetic field of the laser pulse. The laser pulse is kept fairly simple (no chirp) since this suffices to investigate the effects of the bridging atoms on the processes. A Taylor expansion of the first term of Eq. (3) leads to an equivalent expression involving the multipole expansion of the electric and magnetic fields. By keeping only the dominant electric-dipole term we get

$$H^{(2)}(t) = \mathbf{D} \cdot \mathbf{E}_{\rm laser}(t) + \mathbf{S} \cdot \mathbf{B}_{\rm laser}(t), \tag{4}$$

where $\mathbf{E}_{\rm laser}(\mathbf{t})$ and $\mathbf{B}_{\rm laser}(t)$ are the time-dependent electric and magnetic fields of the laser pulse, respectively, and $\mathbf{D}$ the electric-dipole-transition operator.

After having calculated the wavefunctions including SOC and the static magnetic field, we calculate for every many-body-states pair the transition-matrix elements of the operators $\mathbf{D}$ and $\mathbf{S}$ (note that although the spin is not a good quantum number after the inclusion of SOC, one can still calculate its expectation value). These elements interact with the laser pulse giving the time-dependent perturbation term in the Hamiltonian.

In this step, our own codes are implemented for the computation of time propagation during the switch and transfer processes and the optimization of laser pulse as well.[11,13,17,20] By using time-dependent perturbation theory, the many-body wavefunctions are propagated in time in the interaction picture:

$$\frac{\partial c_n}{\partial t} = -\frac{i}{\hbar} \sum_k \langle n|H^{(2)}|k\rangle c_k(t) e^{-i(E_k - E_n)t/\hbar}, \tag{5}$$

where $\langle n|$ and $|k\rangle$ are the unperturned eigenstates, c_n is the complex scalar coefficient of state k in the wave function $\psi(t) = \sum_n c_n(t) e^{-iE_n t/\hbar}|n\rangle$, and E_n and E_k are the energies of state n and k, respectively. The resulting set of the above partial differential equations is solved using an embedded fifth-order Runge-Kutta method combined with the Cash-Karp adaptive step-size control method.[21] In this way we obtain the complete time evolution of the Λ process. In turn the optimal characteristics of the laser pulse and the magnetic field adopted to realize the corresponding ultrafast process can be determined. The optimization of the laser parameters is performed with a self-programmed, largely flexible genetic algorithm.[14]

The geometry of each small system studied here has been theoretically fully optimized within the Hartree-Fock approximation. Energy minimization, which corresponds to zero forces, is considered achieved when the largest force component and the root mean square of all forces are less than 4.5×10^{-4} and 3.0×10^{-4} Hartree/Bohr, respectively. The normal modes and their frequencies are calculated as well in order to confirm the stability of each geometry (absence of imaginary frequencies).

III. RESULTS AND DISCUSSIONS

In the present work different combinations of magnetic centers (Fe, Co, Ni) and nonmagnetic bridging atoms (O, Mg) are considered, which simultaneously satisfy the following three conditions: (i) their electronic ground state is a triplet ground state, (ii) their two magnetic centers are not identical, and (iii) they have a charge of +1. The reason for the latter condition is twofold: first it allows to choose clusters with an even number of electrons (so that triplet states are possible), and second the structures are synthesized by nozzle beam expansion and, of course, the beam should be readily manipulable in experiment. We focus on two combinations of the magnetic centers: Ni-Co and Fe-Co. Since oxygen atoms generally appear in ligand-stabilized structures,[22] we choose O as a preferred *nonmetallic* candidate to connect the two magnetic centers. This is in line with current experimental possibilities (the structures are synthesizable - they are suggested to originate from a monodisperse beam produced by nozzle beam expansion with subsequent mass spectroscopy) and theoretical interest (two prototype bridging atoms chosen). Mg is chosen as an example of *metallic* nonmagnetic bridging atom for comparison to investigate the effect of metallicity of the bridging atom on the spin switching process.

A. O bridge: Spin flip in [Ni-O-Co]$^+$ and [Fe-O-Co]$^+$

As simple starting cases we check the spin-flip and spin-transfer possibilities on the structures [Ni-O-Co]$^+$ and [Fe-O-Co]$^+$, for both of which the geometry-optimization step results in a quasilinear structure. The Ni-O and O-Co bond lengths in the structure [Ni-O-Co]$^+$ are 1.682 Å and 1.917 Å, respectively, and the bond angle is 164°; the Fe-O and O-Co bond lengths in [Fe-O-Co]$^+$ are 1.694 Å and 1.915 Å, respectively, and the bond angle is 175°. However, strictly linear structures have the exactly same symmetry as the dimers ($C_{\infty v}$) and therefore the effects of the bridging

TABLE I. Calculated Mulliken spin density on each atom of the respective linear structures. Only the lowest five triplet states are shown.

Structure	Atom	State 1	State 2	State 3	State 4	State 5
$[Ni\text{-}Co]^+$	Ni	1.924	1.015	1.924	0.025	1.014
	Co	0.076	0.985	0.076	1.975	0.986
$[Ni\text{-}O\text{-}Co]^+$	Ni	1.834	0.846	0.200	0.855	0.497
	O	0.139	0.099	0.047	0.099	0.079
	Co	0.026	1.056	1.754	1.047	1.425
$[Ni\text{-}Mg\text{-}Co]^+$	Ni	1.601	1.621	0.017	0.044	0.045
	Mg	0.379	0.360	-0.022	-0.018	0.528
	Co	0.020	0.019	2.005	1.974	1.427
$[Fe\text{-}Co]^+$	Fe	1.994	1.025	1.994	1.993	1.022
	Co	0.006	0.975	0.006	0.007	0.978
$[Fe\text{-}O\text{-}Co]^+$	Fe	-0.007	1.869	1.936	1.867	1.111
	O	0.008	0.126	0.028	0.113	0.057
	Co	2.000	0.006	0.035	0.021	0.833
$[Fe\text{-}Mg\text{-}Co]^+$	Fe	0.015	0.012	1.975	2.008	1.971
	Mg	0.008	0.008	0.015	-0.012	0.013
	Co	1.978	1.980	0.010	0.003	0.015

atoms are not hidden by the lowering of the symmetry. Additionally, it is relatively easier to locally manipulate the spin in the linear structures due to their weaker magnetic anisotropy. For all these reasons we prefer to use these linear structures as examples to compare with the results obtained from the Mg-bridged structures (see subsection III.B).

The charge distributions obtained from SAC-CI calculations are shown in the left panel of Fig. 2. The Mulliken spin density distribution of these two structures is given in Table I. Some of our previous results for the structures without the bridging atom O are also listed for comparison ($[Ni\text{-}Co]^+$ and $[Fe\text{-}Co]^+$).[23] From the data we can see that the presence of an O atom, to a certain extent, induces a spin-density redistribution. For instance, for the ground state of $[Ni\text{-}O\text{-}Co]^+$, the bridging atom reduces the spin-density maximum on Ni by around 5%; for the second excited state, O relocates the spin-density maximum from Ni to Co; and for the third excited state, O both relocates the spin-density maximum and reduces it by 9%. With respect to the spin localization we can identify two opposite cases: in the fourth state of $[Ni\text{-}Co]^+$ the addition of O practically destroys the spin localization, while in the second state of $[Fe\text{-}Co]^+$ the extra O leads to a well localized spin, thus making the state a candidate for spin-manipulation scenarios. To a smaller extent the spin also becomes more localized in the fifth state of $[Ni\text{-}Co]^+$.

For the structure $[Fe\text{-}Co]^+$ without O atom in-between, two of the five low-lying triplet states exhibit almost equal spin-density distribution on the two magnetic atoms, but these states are not suitable for the Λ process. However, when an O atom bridges Fe and Co, only in the fourth excited triplet state (state 5) the Co atom retains a substantial part of the spin density, which increases the chances for successfully realizing spin-flip and transfer scenarios.

The calculations show that spin flip can be achieved via the Λ process at each magnetic center of these two O-bridged linear structures. That is, spin flips at both the Ni and Co ends of the structure $[Ni\text{-}O\text{-}Co]^+$, as well as at both the Fe and Co ends of the structure $[Fe\text{-}O\text{-}Co]^+$ are possible. Fig. 2 shows three typical spin flip scenarios. For each scenario, the time evolutions of the occupation of the initial (dashed), final (solid), and intermediate (dotted) states involved in the Λ process are plotted in the right panel. Sketches of the respective optimized linear structures, indicating by arrows the specific atom on which spin flip is achieved can be seen in the left panel. Further analysis of the time-resolved expectation values of the spin components (not shown here) shows that the occupation change also corresponds to the spin switching process, since the initial and final states are localized on the same atom but have opposite spin orientations, as shown in Fig. 3.

Another interesting phenomenon is that the population-transfer behaviors with respect to the aforementioned spin-flip scenarios vary substantially across the different magnetic centers (see Fig. 2). For example, Ni seems to behave chaotically during the switching process, Co exhibits a cascade-like behavior, while Fe behaves in a more clear-cut way. In fact, this is counterintuitive because Fe has a more complicated energy-level scheme. However, numerous calculations on structures containing Fe show that this multitude of intragap levels possibly offers more opportunities to search suitable intermediate states for our Λ processes. This finding is consistent with previous results on other linear magnetic structures.[17]

In order to compare the spin flip processes achieved at the same magnetic center but in different systems, the time-resolved expectation values of the spin-angular-momentum components during the spin-flip processes at the Co ends of both structures are plotted in Fig. 4. The spin-flip process at the Co end of $[Fe\text{-}O\text{-}Co]^+$ involves much

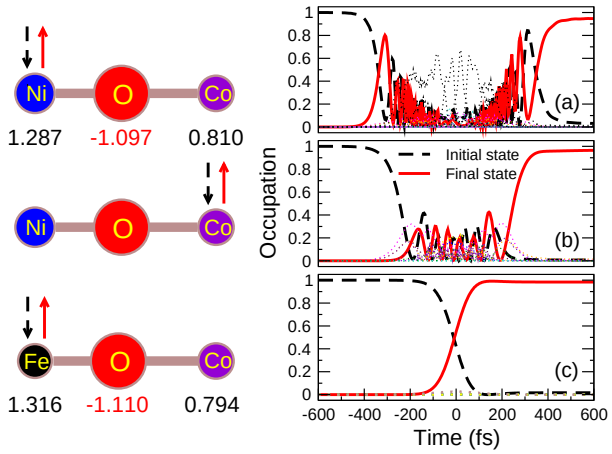

FIG. 2. (Color online) Right panel: local spin flip at the Ni, Co, and Fe ends of the linear structures via the Λ process. (a) Spin flip at the Ni end of $[Ni\text{-}O\text{-}Co]^+$. (b) Spin flip at the Co end of $[Ni\text{-}O\text{-}Co]^+$. (c) Spin flip at the Fe end of $[Fe\text{-}O\text{-}Co]^+$. Left panel: corresponding sketches of the optimized linear structures with arrows indicating the atoms where spin flip occurs. The numbers below the atoms give the atomic charge densities. Figure 3 shows the level schemes as well as the initial and final states of both structures and all three scenarios.

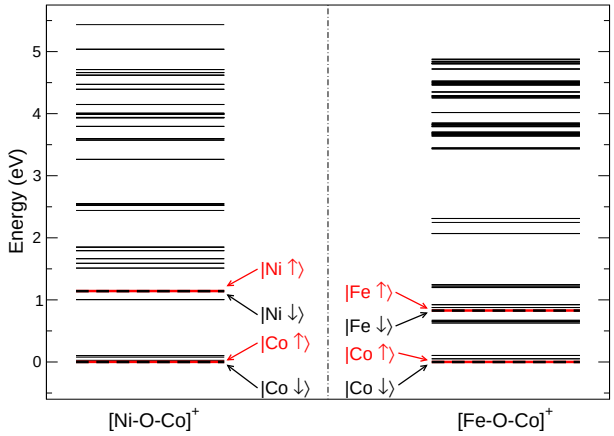

FIG. 3. (Color online) Calculated low-lying energy levels of the structures $[Ni\text{-}O\text{-}Co]^+$ and $[Fe\text{-}O\text{-}Co]^+$ with SOC. In the left panel the initial (black) and the final (red) state for the spin-flip process on the Ni and the Co end of $[Ni\text{-}O\text{-}Co]^+$ (Fig. 2, top and middle panels) are indicated, and in the right panel the initial (black) and the final (red) state for the spin-flip process on the Fe end (Fig. 2, bottom panel), and on the Co end (Fig. 4, bottom panel) of $[Fe\text{-}O\text{-}Co]^+$.

less intermediate states than the process at the Co end of $[Ni\text{-}O\text{-}Co]^+$. The spin also exhibits a higher degree of localization on $[Fe\text{-}O\text{-}Co]^+$ (see Table I). Although the numerous Rabi oscillations taking place in the latter case lower its switching efficiency [Fig. 4(a)], *both* spin-flip processes still complete within less than 500 femtoseconds.

B. Mg bridge: Spin flip in $[Ni\text{-}Mg\text{-}Co]^+$ and $[Fe\text{-}Mg\text{-}Co]^+$

Similar to the O-bridged molecular ions, spin flip can be achieved via the Λ process at each magnetic center of the Mg-bridged structures $[Ni\text{-}Mg\text{-}Co]^+$ and $[Fe\text{-}Mg\text{-}Co]^+$, and the corresponding three typical spin-flip scenarios are shown in Fig. 5. The calculated lowest energy levels of these two Mg-bridged structures with SOC are also shown in Fig. 6 to denote the initial and final states for each spin-flip process. The fully optimized Mg-bridged structures are linear, as shown in the left panel of Fig. 5. Because of the strong metallicity of Mg, the bond lengths in these two structures increase a lot in comparison with the linear, O-bridged structures. More specifically, the Ni-Mg and Mg-Co bond lengths in the structure $[Ni\text{-}Mg\text{-}Co]^+$ are 3.072 Å and 2.765 Å, respectively, and the Fe-Mg and Mg-Co bond lengths in the structure $[Fe\text{-}Mg\text{-}Co]^+$ are 3.217 Å and 2.551 Å, respectively. The increase of the bond length leads to a larger distance between the magnetic atoms (increases around 60% for both cases). Comparing the corresponding

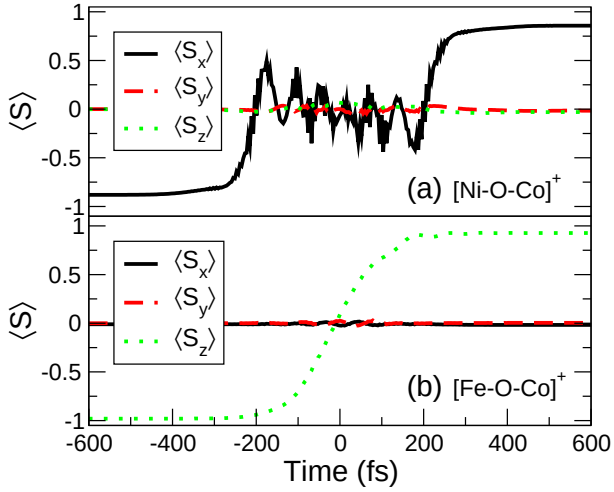

FIG. 4. (Color online) Time-resolved expectation values of the spin angular momentum components during the local spin flip at the Co ends of the linear structures (a) $[Ni\text{-}O\text{-}Co]^+$ (the initial and final states are shown in Fig. 3, left panel) and (b) $[Fe\text{-}O\text{-}Co]^+$ (the initial and final states are shown in Fig. 3, right panel) via the Λ process. Note that in Fig. 2(c) the spin flip is at the Fe end of $[Fe\text{-}O\text{-}Co]^+$.

spin-flip scenarios plotted in Fig. 2 and Fig. 5, we see that this spatial separation seems to have little effect on the ultrafast processes. This is reasonable since spin flip is mainly a local magneto-optic phenomenon at one particular magnetic center, although magnetic-state-dependent spin localization on the intermediate states of the Λ process shows that Mg can temporarily carry some spin density during the processes (in some of the intermediate states the Mg atom carries almost the same spin density as the magnetic atoms).

When Mg bridges the magnetic centers, just like the O case, some spin-density redistribution occurs in the systems, as shown in Table I. Compared with the O case, the Mg atom reduces the maximum of the spin density even stronger. However, Mg has not the same effects on $[Ni\text{-}Co]^+$ and on $[Fe\text{-}Co]^+$: in the former case it lowers the spin density on the Ni atom by around 17% for the ground state (which indicates that the Mg atom can carry some spin in certain states), while for $[Fe\text{-}Co]^+$ it relocates the spin-density maximum from Fe to Co. A general important finding is that the spin density of *all* low electronic states of the Mg-bridged clusters is well localized (at least 70% of the spin density is on one atom), contrary to some electronic states of the non-bridged and the O-bridged clusters.

In addition, a similar tendency of the spin flip scenarios at the Ni, Co, and Fe atoms as in the O-bridged structures also occurs in the present Mg-bridged systems, especially for the clear-cut scenario at the Fe atom. This qualitatively suggests our first rule-of-thumb: In the two-magnetic-center molecular ions, a spin flip at the Fe atom is relatively easier and faster than spin flips at the Ni or Co atoms.

C. Both O and Mg as bridging atoms

If *both* O and Mg are used as bridging atoms simultaneously the resulting geometrically optimized structures are no longer linear but adopt a planar geometry. The sketches of the fully optimized structures $[Ni\text{-}O(Mg)\text{-}Co]^+$ and $[Fe\text{-}O(Mg)\text{-}Co]^+$ are shown in Fig. 7(a) and Fig. 9(a), respectively, and all the interatomic distances are listed in Table II. Taking the structure $[Ni\text{-}O(Mg)\text{-}Co]^+$ as an example, the optimized bond lengths of Ni-O and O-Co are 1.818 Å and 1.928 Å, respectively. Compared with the corresponding values in the linear structure $[Ni\text{-}O\text{-}Co]^+$, both bonds are slightly stretched due to the metallicity of the Mg atom, which results in electron delocalization and thus leads to larger bonds. This is also the case for the structure $[Fe\text{-}O(Mg)\text{-}Co]^+$. The analysis of the spin-density distribution shows that in the low-lying triplet states the spin is mainly localized on the magnetic atoms (Ni, Co, or Fe) and not the bridging atoms (O or Mg). This demonstrates that nonmagnetic bridging atoms do not substantially affect the magnetic character of the magnetic centers. Instead, they can contribute to the magnetic anisotropy of the structure by rearranging the configuration of the magnetic centers and can thus improve the spin transferability.

Figure 7 shows a spin flip scenario at the Co site of the structure $[Ni\text{-}O(Mg)\text{-}Co]^+$ via the Λ process. The pertinent energy levels (mainly triplet states) are given in Fig. 8. It can be seen in Fig. 7(b) that the electronic occupation of the initial and final states undergoes an obvious oscillation when the laser pulse is turned on, which, at the same time, results in the corresponding oscillation of the dominant spin component in Fig. 7(c). Out of the multitude of

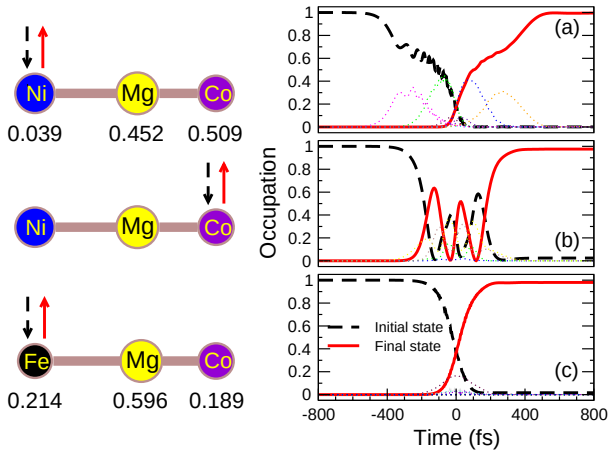

FIG. 5. (Color online) Local spin flip at the Ni, Co, and Fe ends of the structures with Mg as the bridging atom. (a) Spin flip at the Ni end of $[Ni\text{-}Mg\text{-}Co]^+$. (b) Spin flip at the Co end of $[Ni\text{-}Mg\text{-}Co]^+$. (c) Spin flip at the Fe end of $[Fe\text{-}Mg\text{-}Co]^+$. In the left panel the corresponding sketches of the fully optimized structures are shown with arrows indicating of the atoms where spin flip occurs. The numbers below the atoms give their atomic charge densities. Figure 6 shows the level schemes as well as the initial and final states for both structures and all three scenarios.

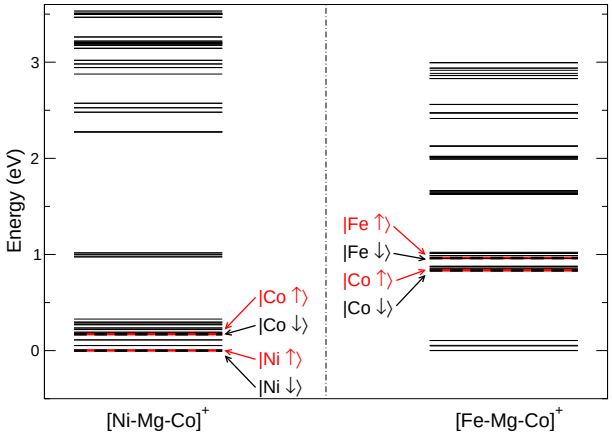

FIG. 6. (Color online) Some of the lowest energy levels of the structures $[Ni\text{-}Mg\text{-}Co]^+$ and $[Fe\text{-}Mg\text{-}Co]^+$ with SOC. In the left panel the initial (black) and the final (red) state for the spin-flip process on the Ni and the Co end of $[Ni\text{-}Mg\text{-}Co]^+$ (Fig. 5, top and middle panels) are indicated, and in the right panel the initial (black) and the final (red) state for the spin-flip process on the Fe end (Fig. 5, bottom panel), and for a very similar spin-flip process on the Co end of $[Fe\text{-}Mg\text{-}Co]^+$ (not shown here).

states included in the propagation one intermediate state carries the majority of the transient electronic population in the spin flip process; this state originates from a triplet state after SOC splitting (see Fig. 8). The energy difference between the initial and final states is around 9.5 cm^{-1}, and the corresponding value between the initial/final states and the main (resonant) intermediate state is around 1.2 eV. Both values satisfy the energy difference requirements for the Λ process and lie within the area marked as ideal in Fig. 1.

As was the case in our previous investigations,[13] spin-transfer scenarios are difficult to realize in two-magnetic-center structures composed of Ni and Co. This is because the energy difference between the relevant electronic states exhibiting spin localization on different atoms is generally too large, making them unsuitable for a Λ process. Substituting Fe for Ni can significantly improve the situation because Fe has more low-energy levels than Ni and it therefore increases the chances of finding a suitable final state with energy close enough to an initial state, whose spin-density is localized on Co. However, from the present work and our previous investigations we conclude that it is extremely difficult to optically transfer the spin in completely linear structures. This brings us to our second rule-of-thumb, i.e. that we need to further lower the symmetry (break the rotational symmetry), as is done for the following structures. As shown in Fig. 9 (b) and (c), both spin flip and spin transfer can be achieved in the structure $[Fe\text{-}O(Mg)\text{-}Co]^+$, although the spin-transfer scenario shown in Fig. 9(c) is not a perfect one. In order to reveal the details of this spin transfer process, the dominant states involved in the Λ process are examined. Fig. 10 shows the

TABLE II. Interatomic distances of the optimized structures [Ni-O(Mg)-Co]$^+$ and [Fe-O(Mg)-Co]$^+$ [see Figs. 7(a) and 9(a)].

Structure [Ni-O(Mg)-Co]$^+$	Interatomic distance (Å)	Structure [Fe-O(Mg)-Co]$^+$	Interatomic distance (Å)
Ni-O	1.818	Fe-O	1.919
Ni-Co	3.346	Fe-Co	3.541
Ni-Mg	2.478	Fe-Mg	2.588
Co-O	1.928	Co-O	1.931
Co-Mg	3.666	Co-Mg	3.600
Mg-O	1.874	Mg-O	1.892

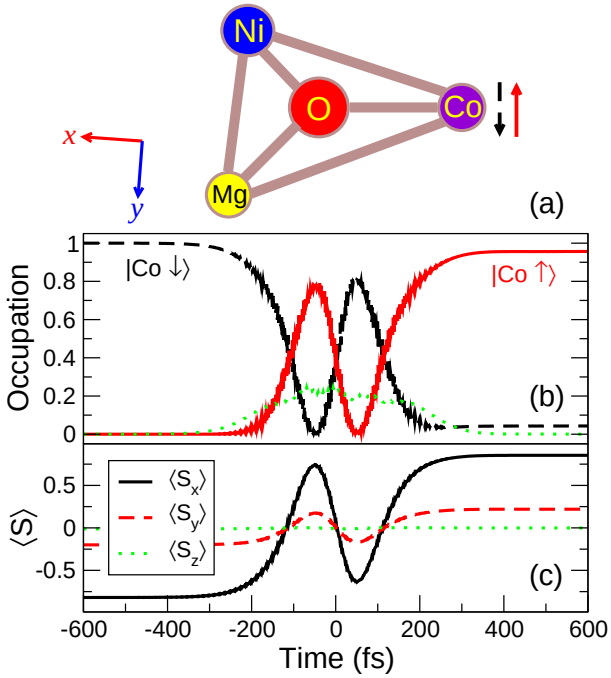

FIG. 7. (Color online) Local spin flip at Co site of the structure [Ni-O(Mg)-Co]$^+$ via the Λ process. (a) Sketch of the optimized geometry with arrows indicating the site where spin flip occurs. (b) Electronic occupation evolutions of the initial (dashed), final (solid), and intermediate (dotted) states during the laser-matter interaction process. (c) Time-resolved expectation values of the spin components.

calculated energy levels of the system. The initial state, the final state of the spin-flip process, and the final state of the spin-transfer process are indicated. Since there are many intermediate states involved in the Λ processes, they are not specified in the level scheme. Table III shows the energies and expectation values of the spin components of the main states involved in the spin transfer process. The corresponding spin localization on specific atoms and the occupation of the final state after the action of the laser pulse are also shown.

The states shown in Table III are labeled in ascending energetic order as obtained from SAC-CI calculations and our self-written programs including SOC. Note that here only the states with occupations of larger than 1% after the influence of the laser pulse are listed. Concerning the spin transfer from Fe to Co, states $|7\rangle$ and $|10\rangle$ are used as the initial and final states, respectively. States $|8\rangle$ and $|9\rangle$ are two of the intermediate states (other intermediate states with higher energies are not listed in Table III). After the laser pulse is gone state $|8\rangle$ still carries some electronic population. The reason is its energetic proximity to the initial state $|7\rangle$, since they both originate from the same triplet state after SOC splitting (see Fig. 10). This has a second consequence as well: state $|8\rangle$ exhibits the same strong spin-density localization on Fe as the initial state $|7\rangle$, and so by retaining some electronic population it impedes spin transfer. This situation could be improved by a proper choice of laser parameters which could block the $|8\rangle \longleftrightarrow |10\rangle$ channel. If we compare the expectation values of the spin component $\langle S_x\rangle$ of state $|7\rangle$ and the spin component $\langle S_z\rangle$ of state $|10\rangle$, we see that this process does not only transfer the spin from Fe to Co but also tilts its direction by almost 90°. This is a completely new spin-manipulation scenario and results from the synergy effects of O *and* Mg as bridging atoms.

TABLE III. Energies and expectation values of the spin angular momentum components of the dominant states involved in the spin transfer scenario from Fe to Co in the structure [Fe-O(Mg)-Co]$^+$(SOC included).

State	Energy (eV)	$\langle S_x \rangle$	$\langle S_y \rangle$	$\langle S_z \rangle$	Spin localization	Occupation of the final states (%)
⋮	⋮	⋮	⋮	⋮	⋮	⋮
$\|10\rangle$	0.3156	-0.006	-0.005	-0.731	Co	72.9
$\|9\rangle$	0.2697	0.000	0.000	0.049	-	1.1
$\|8\rangle$	0.2532	0.862	-0.043	-0.018	Fe	16.2
$\|7\rangle$	0.2529	-0.862	0.043	-0.034	Fe	8.9

D. Parameters of the adopted laser pulses

The laser pulse adopted in the present work is linearly polarized.[12] There is a difference between spin-flip and spin-transfer processes. In the former case, the anisotropy of the molecule influences the spin orientation and then the laser pulse needs to be tilted with respect to the spin. In the latter case, local spin density needs to propagate along the molecular axis and we find that a tilted chain facilitates the process. The laser pulses depend therefore on both the system and the process envisaged. In order to theoretically find suitable laser pulses to achieve the aforementioned spin-flip and spin-transfer Λ processes, a genetic algorithm code has been developed to optimize the parameters of the laser pulse during the light-matter interaction.[14] Table IV shows the laser parameters for each spin-flip or spin-transfer scenario involved in the present work. The main axes of the linear structures are along the z direction, and both the planar structures are approximately in the xy plane. The direction of the external magnetic field with a strength of $|B| = 10^{-5}$ a.u. for each process is also shown in Table IV.

Last but not the least, when we performed simulations on the laser-matter interactions, we have included not only several states but all the magnetic states that obtained from the high-level quantum chemistry calculations (typically more than 150 states). Of course, considering the computational cost, all the states involved in the calculations are below a certain energy cut-off (typically around 2 eV). The genetic algorithm estimates the importance of every included state with respect to transition probabilities and speed, so that only truly participating levels are kept in the calculation. However, because of possible quantum interference effects, the respective thresholds are kept very low, in order not to miss any important channels, typically leading to more than 20 levels included in the actual time propagation. The genetic algorithm also includes states which can be accessed with many-photon processes (typically two), and not only the ones addressable directly from the initial state.

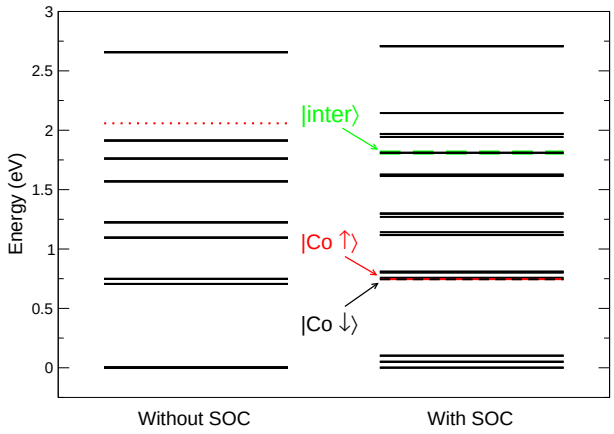

FIG. 8. (Color online) Some of the lowest energy levels of the structure [Ni-O(Mg)-Co]$^+$ without SOC (left side) and with SOC (right side). The red (dotted) state denotes a singlet state and the black (solid) ones represent triplet states. The initial state ($|$Co $\downarrow\rangle$), final state ($|$Co $\uparrow\rangle$), and the intermediate state ($|$inter$\rangle$) that carries the majority of the transient electronic population in the Λ process are indicated as well.

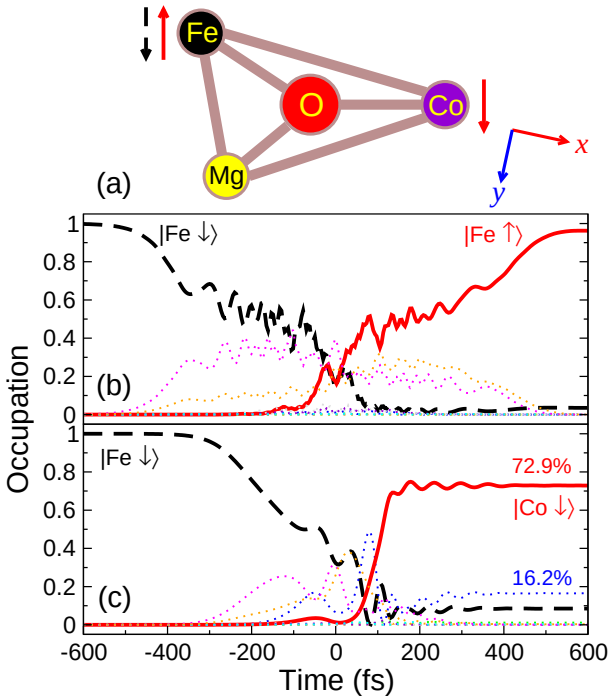

FIG. 9. (Color online) Spin flip and spin transfer processes achieved in the structure [Fe-O(Mg)-Co]$^+$. (a) Sketch of the optimized geometry with arrows indicating the initial and the final spin localization and direction for the spin flip and spin transfer processes. (b) Local spin flip at the Fe site. (c) Spin transfer from Fe to Co.

IV. CONCLUSIONS

Using first-principles theory to describe coherent ultrafast laser-induced Λ processes, the role of the bridging atoms is investigated and is shown to be an important and necessary issue in the study of spin flip/transfer ability in two-magnetic-center molecular ions. In this manuscript, O and Mg are chosen as bridging atoms and their influence is on the spin flip/transfer processes in the charged magnetic molecular ions with two different magnetic centers is studied. The following conclusions can be drawn from the present theoretical calculations:

(i) Spin flip can be readily achieved in the structures with O, Mg, or both as bridging atoms, while spin transfer is promising for some systems. As a first rule-of-thumb the spin flip processes at certain magnetic centers are shown to be easier and more effective in the order Ni (less effective) < Co (moderate) < Fe (more effective).

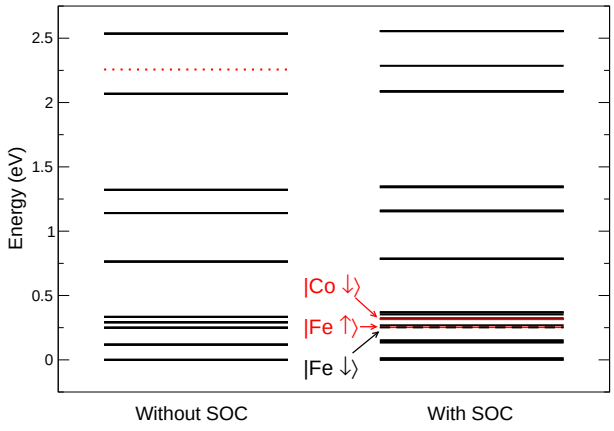

FIG. 10. (Color online) The energy levels of the structure [Fe-O(Mg)-Co]$^+$ without SOC (left side) and with SOC (right side). The red (dotted) state denotes a singlet state and the black (solid) ones are triplet states. The initial state (|Fe ↓⟩), final state for spin flip (|Fe ↑⟩), and the final state for spin transfer (|Co ↓⟩) are specified.

TABLE IV. Optimized parameters of the laser pulse for each spin-flip or spin-transfer process. Here θ and γ denote the angles of incidence in spherical coordinates and ϕ is the angle between the polarization of the light and the plane defined by the propagation direction of the light $\mathbf{k}$ and its projection $\mathbf{k}_{xy}$ on the xy plane. FWHM is the full width at half maximum of the $sech^2$-shaped laser pulse. The directions of the static external magnetic field with a strength of $|B| = 10^{-5}$ a.u. are also shown (Θ and Φ represent its angles in spherical coordinates). Since the linear structures are along the z axis, the γ and Φ angles are irrelevant to them. The orientations of the two planar structures (in the xy plane) are shown in Figs. 7(a) and 9(a). Note that all processes tabulated here refer to single-molecule spin-flip and spin-transfer scenarios.

Structure	Spin process	θ (°)	γ (°)	ϕ (°)	FWHM (fs)	Energy (eV)	Intensity ($\mathrm{Js^{-1}m^{-2}}$)	Θ (°)	Φ (°)
$[\text{Ni-O-Co}]^+$	Flip at Ni	145.2	-	49.2	300.0	3.183	0.262	85.0	-
	Flip at Co	39.9	-	20.8	268.2	2.550	0.262	85.0	-
$[\text{Fe-O-Co}]^+$	Flip at Fe	85.5	-	8.09	300.0	3.828	0.263	85.0	-
	Flip at Co	20.4	-	82.6	238.9	4.822	0.262	85.0	-
$[\text{Ni-Mg-Co}]^+$	Flip at Ni	171.2	-	66.2	300.0	4.804	0.148	5.0	-
	Flip at Co	93.6	-	8.30	300.0	2.079	0.263	5.0	-
$[\text{Fe-Mg-Co}]^+$	Flip at Fe	83.0	-	292.7	300.0	1.486	0.259	85.0	-
	Flip at Co	13.1	-	206.8	268.2	2.068	0.084	85.0	-
$[\text{Ni-O(Mg)-Co}]^+$	Flip at Co	53.7	312.3	268.1	300.0	1.050	4.205	80.0	0.0
$[\text{Fe-O(Mg)-Co}]^+$	Flip at Fe	4.5	89.2	14.3	300.0	1.081	1.046	10.0	0.0
	Transfer Fe→Co	151.4	73.9	282.6	250.5	1.043	0.115	10.0	0.0

(ii) Both bridging atoms O and Mg, to a certain extent, can reduce and relocate the maximum of the atomic spin density. However, in order to improve spin transferability in the investigated linear structures we need to further lower their structural symmetry by introducing O and Mg as bridging atoms simultaneously; this finding constitutes our second rule-of-thumb.

(iii) Extensive calculations show that spins in the linear structures can be flipped more easily, since symmetric structures exhibit a smaller magnetocrystalline anisotropy. However, this is not the case for spin transfer.

(iv) The spin-transfer scenario achieved in $[\text{Fe-O(Mg)-Co}]^+$ shows that the energy differences between the initial, final (where spins are localized at Fe and Co, respectively) and main intermediate states lie within the ideal area for the corresponding requirement in the Λ process. An extra Mg atom attached to O helps to lower the symmetry of the system (second rule-of-thumb), which results in the increase of the efficiency of spin transfer between the involved magnetic centers. Additionally we find a third rule-of-thumb that the combined action of two bridging atoms allows for a spin transfer and a spin tilting of about 90° at the same time. This (up to now unique) Λ process is a new addition to our inventory of possible ultrafast laser-induced spin-manipulation scenarios.

(v) The fact that different parameters of the laser pulse lead to different processes on the same structure (spin-flip or spin-transfer) demonstrates the possibility of coherently controlling spin for applications and, more interestingly, of designing spin-logic devices.

In summary, through systematic quantitative calculations, the present work provides a series of rules-of-thumb for the effects of bridging atoms on the spin-flip and spin-transfer processes in two-magnetic-center molecular ions. These results will serve as a useful reference for future theoretical and experimental investigations.

ACKNOWLEDGMENTS

This work is supported by the National NSF (No. 11002109) of China, the Doctoral Fund (No. 20106102120028) of Ministry of Education of China, NPU Foundation for Fundamental Research (NPU-FFR-JC200935), and NPU Ao-Xiang Star Project. We acknowledge support from the Carl-Zeiss-foundation and the German-Research-Foundation-funded Transregional Collaborative Research Center SFB/TRR 88 "3MET". Part of the calculations was performed in the HPC Center of NPU.

* lichun@nwpu.edu.cn

[1] J. Berezovsky, M. H. Mikkelsen, N. G. Stoltz, L. A. Coldren, and D. D. Awschalom, Science **320**, 349 (2008).
[2] A. M. Kalashnikova, A. V. Kimel, R. V. Pisarev, V. N. Gridnev, A. Kirilyuk, and T. Rasing, Phys. Rev. Lett. **99**, 167205 (2007).
[3] E. Beaurepaire, J.-C. Merle, A. Daunois, and J.-Y. Bigot, Phys. Rev. Lett. **76**, 4250 (1996).
[4] B. Koopmans, J. J. M. Ruigrok, F. Dalla Longa, and W. J. M. de Jonge, Phys. Rev. Lett. **95**, 267207 (2005).
[5] J. Chovan, E. G. Kavousanaki, and I. E. Perakis, Phys. Rev. Lett. **96**, 057402 (2006).
[6] W. Hübner and G. P. Zhang, Phys. Rev. B **58**, R5920 (1998).
[7] G. P. Zhang and W. Hübner, Phys. Rev. Lett. **85**, 3025 (2000).
[8] R. Gómez-Abal, O. Ney, K. Satitkovitchai, and W. Hübner, Phys. Rev. Lett. **92**, 227402 (2004).
[9] M. Schaffry, V. Filidou, S. D. Karlen, E. M. Gauger, S. C. Benjamin, H. L. Anderson, A. Ardavan, G. A. D. Briggs, K. Maeda, K. B. Henbest, F. Giustino, J. J. L. Morton, and B. W. Lovett, Phys. Rev. Lett. **104**, 200501 (2010).
[10] M. N. Leuenberger and D. Loss, Nature **410**, 789 (2001).
[11] W. Hübner, S. P. Kersten, and G. Lefkidis, Phys. Rev. B **79**, 184431 (2009).
[12] G. Lefkidis and W. Hübner, Phys. Rev. B **76**, 014418 (2007).
[13] C. Li, T. Hartenstein, G. Lefkidis, and W. Hübner, Phys. Rev. B **79**, 180413(R) (2009).
[14] T. Hartenstein, C. Li, G. Lefkidis, and W. Hübner, J. Phys. D: Appl. Phys. **41**, 164006 (2008).
[15] G. Lefkidis, G. P. Zhang, and W. Hübner, Phys. Rev. Lett. **103**, 217401 (2009).
[16] G. Lefkidis and W. Hübner, J. Magn. Magn. Mater. **321**, 979 (2009).
[17] T. Hartenstein, G. Lefkidis, W. Hübner, G. P. Zhang, and Y. Bai, J. Appl. Phys. **105**, 07D305 (2009).
[18] H. Nakatsuji *et al.*, http://www.sbchem.kyoto-u.ac.jp/nakatsuji-lab/sacci.html.
[19] M. Frisch *et al.*, Gaussian Inc. Wallingford,CT(2004).
[20] C. Li, F. Yang, G. Lefkidis, and W. Hübner, Acta Phys. Sin. **60**, 017802 (2011).
[21] J. R. Cash and A. H. Karp, ACM Trans. Math. Software **16**, 201 (1990).
[22] G. Lefkidis, C. Li, G. Pal, M. Blug, H. Kelm, H. J. Krüger, and W. Hübner, J. Phys. Chem. A **115**, 1774 (2011).
[23] G. Lefkidis, C. Li, T. Hartenstein, and W. Hübner, J. Phys., Conference Series **200**, 042011 (2010).